Journal of Statistical Physics, Vol. 86, Nos. 5/6, 1997

Universality Properties of the Stationary States in the One-Dimensional Coagulation–Diffusion Model with External Particle Input

Haye Hinrichsen,[1] Vladimir Rittenberg,[2] and Horatiu Simon[2]

Received June 21, 1996

We investigate with the help of analytical and numerical methods the reaction $A + A \to A$ on a one-dimensional lattice opened at one end and with an input of particles at the other end. We show that if the diffusion rates to the left and to the right are equal, for large x, the particle concentration $c(x)$ behaves like $A_s x^{-1}$ (x measures the distance to the input end). If the diffusion rate in the direction pointing away from the source is larger than the one corresponding to the opposite direction, the particle concentration behaves like $A_a x^{-1/2}$. The constants A_s and A_a are independent of the input and the two coagulation rates. The universality of A_a comes as a surprise, since in the asymmetric case the system has a massive spectrum.

KEY WORDS: Nonequilibrium statistical mechanics; reaction–diffusion systems; coagulation model; universality.

1. INTRODUCTION

The study of one-dimensional reaction–diffusion models far from thermal equilibrium is a field of growing interest. The dynamics of these models is characterized by nontrivial correlations, so that ordinary mean-field techniques fail. Therefore theoretical descriptions have to take local fluctuations into account. In general this is a very difficult task and approximation techniques are needed. However, there is a small number of *exactly solvable* models where we can derive exact results. The great interest in solvable models comes from the fact that their physical properties appear also in

[1] Department of Physics of Complex Systems, Weizmann Institute of Science, Rehovot, 76100, Israel.

[2] Physikalisches Institut, Universität Bonn, D-53115, Bonn, Germany.

0022-4715/97/0300-1203$12.50/0

many other, more complicated models. If we consider one-dimensional two-state models (i.e., models with only one species of particles), there are only two classes of exactly solvable systems. The first class includes diffusion (or exclusion) models, which are solvable by means of Bethe ansatz techniques. The second class contains mainly models with an underlying theory of free fermions. The most important representative of this class is the so-called coagulation model, which is the subject of the present work.

Coagulation models describe particles which diffuse stochastically in a d-dimensional space. When two particles meet at the same place they coalesce to a single one ($A + A \to A$). For a possible experimental realization see ref. 1. The theoretical study of coagulation models has a long history. It started with the observation that the critical dimension of the corresponding field theory is $d_c = 2$.[2] A breakthrough toward the exact solution of the one-dimensional coagulation model on a lattice was the introduction of so-called interparticle distribution functions (IPDFs).[3] For certain reaction–diffusion processes the IPDF formalism leads to a hierarchy of decoupled differential equations similar to those obtained for the Glauber model.[4] The most general conditions for the decoupling to occur as well as the cases when the underlying Hamiltonian can be diagonalized in terms of free fermions are given in ref. 5. A variety of exact solutions were found for the coagulation model with or without backreaction (decoagulation $A \to A + A$).[3]

The one-dimensional coagulation model with spatial *homogeneous* external particle input at all sites has been studied extensively[6] and algebraic relaxation times have been observed. In this paper we investigate the same model with open boundary conditions and *localized* particle input at the ends of the chain, which was considered for the first time in the mean-field approximation in ref. 7. In the present work we compute the particle concentration in the stationary state. We give the full solution on the lattice and in the continuum. The main motivation of this paper stems from the observation that in the mean-field approximation (to be reviewed later) the density of particles has an algebraic decay and one can see if one has universality properties.

The coagulation model studied in this paper is defined as follows. Particles of one species diffuse stochastically on a linear one-dimensional lattice with L sites. The diffusion may be biased due to some external force. If two particles meet at the same site, they coalesce to a single one. In addition, particles are added stochastically with a given probability at the endpoints of the lattice. We use random sequential updates, i.e., we assume continuous time evolution which is described by a linear master equation. Altogether the dynamics is defined by the six nearest neighbor processes with rates shown in Fig. 1.

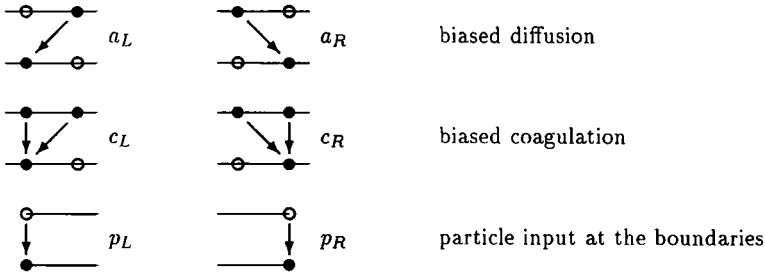

Fig. 1. Bulk and boundary processes in the coagulation–diffusion model.

The master equation for a lattice of L sites can be written in a compact form by (for notations see ref. 8)

$$\frac{\partial}{\partial t}|P(t)\rangle = -H\,|P(t)\rangle \tag{1.1}$$

where the vector $|P(t)\rangle$ denotes the probability distribution. H is the time evolution operator, which can be written as a sum of nearest neighbor reaction matrices $H_{n,n+1}$ plus two further matrices for particle input I_L and I_R:

$$H = I_L + I_R + \sum_{n=1}^{L-1} H_{n,n+1} \tag{1.2}$$

In the canonical basis of particle configurations ($|\varnothing\varnothing\rangle$, $|\varnothing A\rangle$, $|A\varnothing\rangle$, $|AA\rangle$) these matrices read

$$H_{n,n+1} = \begin{pmatrix} 0 & 0 & 0 & 0 \\ 0 & a_L & -a_R & -c_R \\ 0 & -a_L & a_R & -c_L \\ 0 & 0 & 0 & c_L + c_R \end{pmatrix}_{n,n+1} \tag{1.3}$$

and

$$I_L = \begin{pmatrix} p_L & 0 \\ -p_L & 0 \end{pmatrix}_1, \qquad I_R = \begin{pmatrix} p_R & 0 \\ -p_R & 0 \end{pmatrix}_L \tag{1.4}$$

It is useful to introduce some notations:

$$\begin{aligned} r &= \frac{2(a_R - a_L)}{a_R + a_L}, & s &= \frac{2(c_R + c_L)}{a_R + a_L} \\ t &= \frac{2(c_R - c_L)}{a_R + a_L}, & q &= \left(\frac{a_R}{a_L}\right)^{1/2} \end{aligned} \tag{1.5}$$

$c(i)$ denotes the particle concentration at the site i. When we will consider the continuum limit (the lattice spacing $\lambda \to 0$), we will use the notation

$$\rho(x) = \lambda^{-1} c\left(\frac{i}{\lambda}\right), \qquad \hat{r} = \frac{r}{\lambda}, \qquad \hat{s} = \frac{s}{\lambda}, \qquad \hat{p} = \frac{p_L}{\lambda^2} \tag{1.6}$$

Before we give our results we remind the reader of the results of the improved mean-field calculations.[7] Assuming that the coagulation rate $\hat{s}$ is proportional to the concentration $\hat{s} = \zeta\rho(x)$, for large values of x (we take $p_R = 0$ and the source is at $x = 0$), the densities are

$$\begin{aligned} &q < 1 \quad \text{(bias to the left):} && \rho(x) \propto \exp(-|\hat{r}|\, x) \\ &q = 1 \quad \text{(symmetric diffusion):} && \rho(x) \approx (2/\zeta)^{1/2}\, x^{-1} \\ &q > 1 \quad \text{(bias to the right):} && \rho(x) \approx (\hat{r}/2\zeta)^{1/2}\, x^{-1/2} \end{aligned} \tag{1.7}$$

Notice the algebraic falloff for $q \geqslant 1$.

The IPDF method is applicable if

$$a_R = c_R = q, \qquad a_L = c_L = q^{-1} \tag{1.8}$$

These conditions are equivalent to $r = t$ and $s = 2$. This will also be called the fermionic case (the Hamiltonian can be diagonalized in terms of free fermions[5,9,10]). The special case $q = 1$, $p_R = p_L = \infty$ was already studied in a paper by Derrida *et al.*[11] which was a source of inspiration for the present work. We list now our main results in the $p_R = 0$ case:

(a) *Lattice in the thermodynamic limit* (j fixed, $L \to \infty$):

$$c(j) = \frac{2}{\pi j} + \frac{1}{\pi j^2} - \frac{1}{2\pi j^4} + \left(\frac{3}{8\pi} - \frac{12}{\pi p_L^2}\right)\frac{1}{j^5} + O(j^{-6}), \qquad q = 1 \tag{1.9}$$

$$c(j) = \sqrt{\frac{q^2-1}{(q^2+1)\,\pi j}}\left[1 + \left(\frac{3q^4+20q^2-1}{8(q^4-1)} - \frac{(q^2-1)^3}{2q^2(q^2+1)\,p_L^2}\right)\frac{1}{j}\right] + O(j^{-5/2}), \qquad q > 1 \tag{1.10}$$

$$c(j) = q^{4j}\left(\sqrt{\frac{1-q^2}{(q^2+1)\,\pi j}} + O(j^{-3/2})\right), \qquad q < 1 \tag{1.11}$$

Several exact values for $c(j)$ are given in Appendix A.

(b) *Continuum and thermodynamic limit* (x fixed, $L \to \infty$):

$$\rho(x) = \frac{2}{\pi x} - \frac{12}{\pi \hat{p}^2 x^5} + \frac{5040}{\pi \hat{p}^4 x^9} + O(\hat{p}^{-6} x^{-13}), \qquad q = 1 \quad (1.12)$$

$$\rho(x) = \sqrt{\frac{\hat{r}}{2\pi x}} + \frac{1}{4\sqrt{2\pi \hat{r}}} \left(\frac{11}{2} - \frac{\hat{r}^4}{\hat{p}^2} \right) \frac{1}{x^{3/2}} + O(x^{-5/2}), \qquad q > 1 \quad (1.13)$$

(c) *Continuum and scaling limit* ($z = x/L$ fixed, $L \to \infty$, $q = 1$):

$$\lim_{\substack{L \to \infty \\ x \to \infty \\ z = x/L \text{ fixed}}} L\rho(x) = \Phi(z) \quad (1.14)$$

$$\Phi(z) = \frac{\sinh(\pi z) + \sin(\pi z)}{\cosh(\pi z) - \cos(\pi z)} + \sum_{k=1}^{+\infty} \left\{ \frac{\sinh[2\pi(z/2 - k)] + \sin(\pi z)}{\cosh[2\pi(z/2 - k)] - \cos(\pi z)} + (k \leftrightarrow -k) \right\} \quad (1.15)$$

As a by-product, the one-hole functions are also obtained. This result is not trivial, since they represent two-point correlation functions.

In the long Section 2 and in Appendices A and B these results are derived. Many of our calculations are extensions of results obtained in refs. 9 and 10, from which we borrow the notations. Also in Section 2 we give the spectrum of the Hamiltonian in the one-hole sector. For $q \neq 1$ the spectrum is massive in spite of the algebraic behavior seen in Eqs. (1.10) and (1.13). For $q = 1$ most of the excitations are massless (they coincide with those of the open chain, $p_L = 0$), but there are also some massive excitations with a mass given by p_L. In many systems timelike and spacelike properties seem to be coupled in the sense that long-range correlations in time imply long-range correlations in space. This is not necessary valid for stochastic models which are not isotropic. As we will see in this model, one can have short-range correlations in time, but long-range correlations in space (for another example, see ref. 8).

In Section 3 we consider the problem of the universality of the coefficients $2/\pi$ for the leading contribution in the $q = 1$ case [see Eqs. (1.9) and (1.12)] and of $[(q^2 - 1)/(q^2 + 1)\,\pi]^{1/2}$ for $q > 1$ [see Eqs. (1.10) and (1.13)] as well as of the finite-size scaling function (1.15). For this purpose we keep the definition $\sqrt{a_R/a_L} = q$, but leave the coagulation rates c_R and c_L

arbitrary. For the open chain (no input) the spectra are known to be massless for $q=1$ and massive for $q>1$.[8] The modifications introduced by the boundary terms are supposed not to change radically the picture. Using Monte Carlo simulations (the details are given in Appendix C), we show that indeed for several values of c_L and c_R the expansion coefficients as well as the finite-size scaling functions are universal.

The reader not interested in lengthy calculations can skip Section 2 and proceed directly to Section 3.

2. EXACT SOLUTION IN THE $a_R=c_R=q$, $a_L=c_L=q^{-1}$ CASE

2.1. Finite-Lattice Calculations

In this section we give the full solution of the coagulation model with particle input at the boundaries. We use the IPDF formalism[3] in which the whole problem is formulated in terms of probabilities for finding sequences of unoccupied sites (holes). In this basis the master equation leads to a hierarchy of sets of equations according the number of holes. It is known[5] that these sets decouple from the higher ones provided that the rates for diffusion and coagulation coincide. Therefore the one-hole sector decouples from the higher sectors and can be solved separately. In what follows we will assume that the above condition holds.

For completeness we will consider the model with input at the left end (rate p_L) and right end (rate p_R).[3] We will actually show that by solving the problem with $p_R=0$ one can obtain the general solution $p_R\neq 0$. Although in principle feasible, we did not look at the case when one also has output of particles at both ends.

Although not obviously needed for the study of the stationary state, we will also give the spectrum of the problem in the one-hole sector for two reasons. One is technical: the eigenfunctions and eigenvalues occur in the expression of the stationary-state hole probabilities. The second one is related to the physical significance of our result: it is important to know when one has massless or massive excitations.

Let $\Omega(j, m, t)$ denote the probability to find the sites $j+1, j+2, \ldots, m$ empty at time t. By a careful analysis of the elementary processes taking place at the edges of the hole one is led to the following equations of motion for the one-hole sector:

[3] In order to avoid confusion in terminology we give in parentheses alternative usages in the literature: periodic boundary conditions (model on a ring), open boundary conditions (linear chain with closed ends), open boundary with particle input (chain with open ends).

- For holes which do not touch the boundaries $(0 < j < m < L)$:

$$\frac{d}{dt}\Omega(j, m, t) = q\Omega(j-1, m, t) + q^{-1}\Omega(j+1, m, t) + q\Omega(j, m-1, t) + q^{-1}\Omega(j, m+1, t) - 2(q+q^{-1})\,\Omega(j, m, t) \tag{2.1}$$

- For holes touching the left boundary $(0 = j < m < L)$:

$$\frac{d}{dt}\Omega(0, m, t) = q\Omega(0, m-1, t) + q^{-1}\Omega(0, m+1, t) - (q+q^{-1}+p_L)\,\Omega(0, m, t) \tag{2.2}$$

- For holes touching the right boundary $(0 < j < m = L)$:

$$\frac{d}{dt}\Omega(j, L, t) = q\Omega(j-1, L, t) + q^{-1}\Omega(j+1, L, t) - (q+q^{-1}+p_R)\,\Omega(j, L, t) \tag{2.3}$$

- For the hole extending over the whole chain $(j = 0,\ m = L)$:

$$\frac{d}{dt}\Omega(0, L, t) = -(p_L + p_R)\,\Omega(0, L, t) \tag{2.4}$$

In these equations we have taken $\Omega(j, j, t) = 1$. This leads to an *inhomogeneous* system of equations. Separating the time dependence and introducing rescaled probabilities

$$\Omega(j, m, t) = e^{-\Lambda t} q^{+j+m} \tilde{\Omega}(j, m) \tag{2.5}$$

we obtain the simplified system of equations

$$(2(q+q^{-1}) - \Lambda)\,\tilde{\Omega}(j, m) = \tilde{\Omega}(j-1, m) + \tilde{\Omega}(j+1, m) + \tilde{\Omega}(j, m-1) + \tilde{\Omega}(j, m+1) \tag{2.6}$$

$$(q+q^{-1}+p_L-\Lambda)\,\tilde{\Omega}(0, m) = \tilde{\Omega}(0, m-1) + \tilde{\Omega}(0, m+1) \tag{2.7}$$

$$(q+q^{-1}+p_R-\Lambda)\,\tilde{\Omega}(j, L) = \tilde{\Omega}(j+1, L) + \tilde{\Omega}(j-1, L) \tag{2.8}$$

$$(p_L + p_R - \Lambda)\,\tilde{\Omega}(0, L) = 0 \tag{2.9}$$

which the inhomogeneous boundary condition $\tilde{\Omega}(j, j) = q^{-2j}$.

The *homogeneous* set of solutions describes the relaxational modes of the system. It is obtained by setting $\tilde{\Omega}(j, j) = 0$ and can be computed easily by using similar techniques as in ref. 9, which rely mainly on the invariance of the bulk equation (2.1) under reflections $j \leftrightarrow m$ and $j \leftrightarrow L - m$. Denoting

$$g(j, z) = \frac{\sinh[j \operatorname{arcsinh} \frac{1}{2}(q + q^{-1} - z)]}{\sinh[L \operatorname{arcsinh} \frac{1}{2}(q + q^{-1} - z)]} \tag{2.10}$$

we find the homogeneous solutions

$$\Phi_0(j, m) = g(L-j, p_L)\, g(m, p_R) - g(L-m, p_L)\, g(j, p_R) \tag{2.11}$$

$$\Phi_k^{(L)}(j, m) = \sin\frac{\pi k j}{L}\, g(L-m, p_L) - \sin\frac{\pi k m}{L}\, g(L-j, p_L) \tag{2.12}$$

$$\Phi_k^{(R)}(j, m) = \sin\frac{\pi k j}{L}\, g(m, p_R) - \sin\frac{\pi k m}{L}\, g(j, p_R) \tag{2.13}$$

$$\Phi_{k,l}(j, m) = \sin\frac{\pi k j}{L} \sin\frac{\pi l m}{L} - \sin\frac{\pi k m}{L} \sin\frac{\pi l j}{L} \tag{2.14}$$

They have the excitation energies

$$\Lambda_0 = p_L + p_R \tag{2.15}$$

$$\Lambda_k^{(L)} = q + q^{-1} + p_L - 2\cos\frac{\pi k}{L} \tag{2.16}$$

$$\Lambda_k^{(R)} = q + q^{-1} + p_R - 2\cos\frac{\pi k}{L} \tag{2.17}$$

$$\Lambda_{k,l} = 2(q + q^{-1}) - 2\cos\frac{\pi k}{L} - 2\cos\frac{\pi l}{L} \tag{2.18}$$

where $1 \leqslant k < l \leqslant L$. In contrast to the coagulation model without particle input ($p_R = p_L = 0$), where the spectrum is massless for $q = 1$ and massive otherwise (q real), in the case of particle input the spectrum is more complex. Even for $q = 1$, where most of the excitations are massless [Eq. (2.18)], we get some massive ones, too [Eqs. (2.15)–(2.17)].

The derivation of the *inhomogeneous* (steady-state) solution is more difficult. For symmetric coagulation on a ring with infinite particle input at a single site an exact solution has been found recently in refs. 11 and 12. This solution applies to an open chain with symmetric diffusion ($q = 1$) and

infinite particle input at both ends ($p_L = p_R = \infty$). It is given by $\tilde{\Omega}(j, j) = 1$ and

$$\tilde{\Omega}(j, m) = \frac{8}{L^2} \sum_{k,l=1}^{L-1}{}' \frac{\sin\frac{\pi k}{L} \sin\frac{\pi l}{L} \left(\sin\frac{\pi kj}{L} \sin\frac{\pi lm}{L} - \sin\frac{\pi km}{L} \sin\frac{\pi lj}{L} \right)}{\left(\cos\frac{\pi l}{L} - \cos\frac{\pi k}{L} \right) \left(2 - \cos\frac{\pi k}{L} - \cos\frac{\pi l}{L} \right)}$$

$$(j < m) \tag{2.19}$$

where the prime indicates that the sum runs only over even values of k and odd values of l. Formally this solution can be expressed in terms of the two-particle excitations (2.14) by

$$\tilde{\Omega}(j, m) = \frac{8}{L^2} \sum_{k,l=1}^{L-1}{}' \frac{f_{k,l} \Phi_{k,l}(j, m)}{\Lambda_{k,l}} \tag{2.20}$$

where

$$f_{k,l} = \frac{1}{2} [1 - (-)^{k+l}] \frac{\sin(\pi k/L) \sin(\pi l/L)}{\cos(\pi l/L) - \cos(\pi k/L)} \tag{2.21}$$

plays the role of a structure function. However, we proved that the general stationary solution for the asymmetric diffusion and finite particle input rates has the same structure and differs only in the structure function $f_{k,l}$. This function can be derived as follows. Let us symbolize a contraction of two functions over momentum indices k, l by $\langle \cdot, \cdot \rangle_{k,l}$ and similarly a contraction over spatial indices by $\langle \cdot, \cdot \rangle_{j,m}$. Then Eq. (2.20) reads $\tilde{\Omega} = \langle f, \Phi/\Lambda \rangle_{k,l}$ and therefore the application of the discrete Laplacian $\Delta\Phi = \Lambda\Phi$ yields $\Delta\tilde{\Omega} = \langle f, \Phi \rangle_{k,l}$, which is zero everywhere except at the boundaries. Using the orthogonality relation $\langle \Phi_{k,l}, \Phi_{k',l'} \rangle_{j,m} \sim \delta_{k,k'} \delta_{l,l'}$, one can therefore compute f by

$$f \sim \langle f, \delta\delta \rangle_{k,l} \sim \langle f, \langle \Phi, \Phi \rangle_{j,m} \rangle_{k,l} \sim \langle \langle f, \Phi \rangle_{k,l}, \Phi \rangle_{j,m} \sim \langle \Delta\tilde{\Omega}, \Phi \rangle_{j,m} \tag{2.22}$$

Carrying out these contractions, it turns out that the structure function f consists of three parts

$$f_{k,l} = f_{k,l}^{(\infty)} + f_{k,l}^{(L)} + f_{k,l}^{(R)} \tag{2.23}$$

The first part $f_{k,l}^{(\infty)}$ describes the asymmetric coagulation model with infinite particle input rates at *both* ends. It is given by

$$f_{k,l}^{(\infty)} = [1-(-)^{k+l}q^{-2L}] \times \frac{(q+q^{-1})^2 \sin\frac{\pi k}{L}\sin\frac{\pi l}{L}\sin\frac{\pi(k+l)}{2L}\sin\frac{\pi(k-l)}{2L}}{\left(q^2+q^{-2}-2\cos\frac{\pi(k+l)}{L}\right)\left(q^2+q^{-2}-2\cos\frac{\pi(k-l)}{L}\right)} \tag{2.24}$$

For $q \to 1$ (symmetric diffusion) this expression reduces to Eq. (2.21). The other two parts depend on the input rates p_L, p_R and read

$$f_{k,l}^{(L)} = \frac{\sin\frac{\pi k}{L}\sin\frac{\pi l}{L}\left(\cos\frac{\pi l}{L}-\cos\frac{\pi k}{L}\right)}{2\left(q+q^{-1}+p_L-2\cos\frac{\pi k}{L}\right)\left(q+q^{-1}+p_L-2\cos\frac{\pi l}{L}\right)} \tag{2.25}$$

$$f_{k,l}^{(R)} = \frac{(-)^{k+l+1}q^{-2L}\sin\frac{\pi k}{L}\sin\frac{\pi l}{L}\left(\cos\frac{\pi l}{L}-\cos\frac{\pi k}{L}\right)}{2\left(q+q^{-1}+p_R-2\cos\frac{\pi k}{L}\right)\left(q+q^{-1}+p_R-2\cos\frac{\pi l}{L}\right)} \tag{2.26}$$

The inhomogeneous solution of the difference equations (2.6)–(2.9) is then obtained by inserting Eq. (2.23) into Eq. (2.20).

For a fixed value of the lattice length L the hole probability function depends on three parameters: p_L, p_R, and q. By reversing the ends of the lattice, one sees that

$$\Omega(j, m, p_L, p_R, q) = \Omega(L-m+1, L-j+1, p_R, p_L, q^{-1}) \tag{2.27}$$

Due to (2.23), the hole probability function obeys the rule

$$\begin{aligned}\Omega(j, m, p_L, p_R, q) &= \Omega(j, m, p_L, 0, q) + \Omega(L-m+1, L-j+1, p_R, 0, q^{-1}) \\ &\quad - \Omega(j, m, 0, 0, q)\end{aligned} \tag{2.28}$$

Therefore it will be sufficient to study systems with particle input at only one boundary. Using (2.28), one can relate physical quantities referring to systems with particle input at both ends with the ones computed for

systems for which p_L or p_R is 0. As an example, the particle concentration at site j

$$c(j) = 1 - \Omega(j-1, j) \tag{2.29}$$

can be written as a sum (2.28):

$$c(j, p_L, p_R, q) = c(j, p_L, 0, q) + c(L-j+1, p_R, 0, q^{-1}) - c(j, 0, 0, q) \tag{2.30}$$

Here $c(j, 0, 0, q)$ is the particle concentration in the stationary state for input rates 0, i.e., it is the particle concentration of one random walker occupying the whole lattice (2.74).

2.2. The Thermodynamic Limit

The formulas derived in the last section are exact solutions for finite chains. We consider the thermodynamic limit. In this limit the right boundary is moved to infinity while the observer stays at a fixed distance j from the left boundary. We consider systems with no particle input at the right end ($p_R = 0$). We are left with only two parameters, namely the input rate at the left boundary $p \equiv p_L$ and the asymmetry parameter q. Carrying out the limit $L \to \infty$ in Eqs. (2.23)–(2.26), one is led to a simple integral representation of the one-hole probabilities $\Omega(j, m)$. To this end it is convenient to introduce the quantities μ_z,

$$\mu_z = \tfrac{1}{2}(q + q^{-1} - iz) - \sqrt{\tfrac{1}{4}(q + q^{-1} - iz)^2 - 1} \tag{2.31}$$

and its inverse

$$\mu_z^{-1} = \tfrac{1}{2}(q + q^{-1} - iz) + \sqrt{\tfrac{1}{4}(q + q^{-1} - iz)^2 - 1} \tag{2.32}$$

Using this notation, we express the one-hole probabilities in the thermodynamic limit by the elliptic integral

$$\Omega(j, m) = 1 - \frac{q^{j+m}}{2\pi i} \int_{-\infty}^{+\infty} dz \left(\frac{1}{z} - \frac{z}{z^2 + p^2} \right) (\mu_z^j \mu_{-z}^m - \mu_z^m \mu_{-z}^j) \tag{2.33}$$

A proof of this formula is given in Appendix A, where also the particle concentration at the first few sites for infinite input rate is computed

exactly. Let us now investigate the asymptotic behavior of the particle concentration

$$c(j)=\frac{1}{2\pi iq}\int_{-\infty}^{+\infty} dz\,(q^2\mu_z\mu_{-z})^j\left(\frac{1}{z}-\frac{z}{z^2+p^2}\right)(\mu_z^{-1}-\mu_{-z}^{-1}) \tag{2.34}$$

for large j. Three cases have to be considered separately:

2.2.1. Symmetric Case ($q=1$). For $q=1$ the expression $\log(\mu_z\mu_{-z})$ in Eq. (2.34) can be expanded in first order by

$$\log(\mu_z\mu_{-z})=-\sqrt{2\,|z|}+O(z^{3/2}) \tag{2.35}$$

Rewriting the integral (2.34) by

$$c(j)=\frac{1}{2\pi i}\int_{-\infty}^{+\infty} dz\,\exp(-\sqrt{2\,|z|}\,j)\,r(j,z) \tag{2.36}$$

$$r(j,z)=\exp(\sqrt{2\,|z|}\,j)(\mu_z\mu_{-z})^j\left(\frac{1}{z}-\frac{z}{z^2+p^2}\right)(\mu_z^{-1}-\mu_{-z}^{-1}) \tag{2.37}$$

and expanding $r(j,z)$ in z, we can solve the integral order by order. We obtain the series

$$c(j)=\frac{2}{\pi j}+\frac{1}{\pi j^2}-\frac{1}{2\pi j^4}+\left(\frac{3}{8\pi}-\frac{12}{\pi p^2}\right)\frac{1}{j^5}+O(j^{-6}) \tag{2.38}$$

This proves that in the fermionic case the first three terms in the large-x expansion are independent of the input rate p.

2.2.2. Bias to the Right ($q>1$). In this case we find that the expression $\log(q^2\mu_z\mu_{-z})$ in Eq. (2.34) can be expanded in first order by

$$\log(q^2\mu_z\mu_{-z})=-q^2\frac{q^2+1}{(q^2-1)^3}z^2-O(z^4) \tag{2.39}$$

Rewriting the integral (2.34) by

$$c(j)=\frac{1}{2\pi iq}\int_{-\infty}^{+\infty} dz\,\exp\left(-q^2\frac{q^2+1}{(q^2-1)^3}jz^2\right)s(j,z) \tag{2.40}$$

$$s(j,z)=\exp\left(q^2\frac{q^2+1}{(q^2-1)^3}jz^2\right)\left(\frac{1}{z}-\frac{z}{z^2+p^2}\right)$$
$$\times(q^2\mu_z\mu_{-z})^j(\mu_z^{-1}-\mu_{-z}^{-1}) \tag{2.41}$$

and expanding $s(j, z)$ in z, we can again solve the integral order by order. We obtain

$$c(j) = \sqrt{\frac{q^2-1}{(q^2+1)\,\pi j}}\left[1 + \left(\frac{3q^4+20q^2-1}{8(q^4-1)} - \frac{(q^2-1)^3}{2q^2(q^2+1)\,p^2}\right)\frac{1}{j}\right] + O(j^{-5/2}) \tag{2.42}$$

We notice that, as opposed to the symmetric case, only the leading term is independent of the input rate.

2.2.3. Bias to the Left $q < 1$. If the particles hop preferentially to the left, they accumulate at the left boundary and thus we expect an exponential decay of the concentration profile. In fact, as can be seen from Eq. (2.34), the expression $q^{2j-1}c(j)$ is invariant under the replacement $q \to q^{-1}$. This means that for a bias directed toward the left boundary the concentration profile decays like $q^{4j}j^{-1/2}$:

$$c(j) = q^{4j}\left(\sqrt{\frac{1-q^2}{(q^2+1)\,\pi j}} + O(j^{-3/2})\right) \tag{2.43}$$

We remark that the series presented in this section are *asymptotic series* since they are derived from an elliptic integral.

2.3. The Continuum Limit

An alternative way to describe the physics of the coagulation model with an external input source is to consider the continuum limit of the one-hole equations. This can be done by taking the lattice spacing $\lambda \to 0$ while keeping the two quantities

$$\hat{r} = \frac{2(q-q^{-1})}{\lambda(q+q^{-1})} \qquad \text{and} \qquad \hat{p} = \frac{2p_L}{\lambda^2(q+q^{-1})} \tag{2.44}$$

constant. We then replace the empty-hole probabilities $\Omega(x, y)$ by their continuous counterparts:

$$\Omega^c(x, y) = \Omega\left(\frac{j}{\lambda}, \frac{m}{\lambda}\right) \tag{2.45}$$

It is useful to rescale the hole density function taking $\hat{\Omega}(x, y) = \Omega^c(x, y)$ $\exp[-\frac{1}{2}\hat{r}(x+y)]$, which satisfies the equation [see Eq. (2.6)]

$$(\Delta - \tfrac{1}{2}\hat{r}^2)\,\hat{\Omega}(x, y) = 0 \qquad (L > y > x > 0) \tag{2.46}$$

By solving the continuous counterparts of Eqs. (2.2)–(2.4), we determined the value of the hole density function on the boundaries. The solutions are:

- Along the left boundary ($x=0$, $0 \leqslant y \leqslant L$):

$$\hat{\Omega}(0, y) = \begin{cases} \dfrac{\sinh[(L-y)\sqrt{t^2/4+\hat{p}}]}{\sinh[L\sqrt{t^2/4+\hat{p}}]} & \text{if } \hat{p} \neq \infty \\ 0 & \text{if } \hat{p} = \infty \end{cases} \tag{2.47}$$

- Along the upper boundary ($y=L$, $0 \leqslant x \leqslant L$):

$$\hat{\Omega}(x, L) = \begin{cases} \dfrac{[\exp(-\hat{r}L)]\sinh(\frac{1}{2}\hat{r}x)}{\sinh(\frac{1}{2}\hat{r}L)} & \text{if } \hat{r} \neq 0 \\ x/L & \text{if } \hat{r} = 0 \end{cases} \tag{2.48}$$

- On the diagonal ($0 \leqslant x = y \leqslant L$) the normalization condition is

$$\hat{\Omega}(x, x) = \exp(-\hat{r}x) \tag{2.49}$$

Equation (2.46) together with the boundary conditions (2.47)–(2.49) define a Dirichlet problem for the function $\hat{\Omega}(x, y)$. The formal solution is

$$\hat{\Omega}(x, y) = \oint_C ds\, \hat{\Omega}(x', y') \frac{\partial}{\partial n} \mathcal{G}(x, y, x', y') \tag{2.50}$$

where C is the contour along the boundaries, $\partial/\partial n$ is the normal derivative, and $\mathcal{G}(x, y, x', y')$ is the Green function defined by

$$(\Delta - \tfrac{1}{2}\hat{r}^2)\, \mathcal{G}(x, y, x', y') = \delta(x-x')\, \delta(y-y') \tag{2.51}$$

$$\mathcal{G}(0, y, x', y') = \mathcal{G}(x, y, 0, y') = \mathcal{G}(x, L, x', y') = \mathcal{G}(x, y, x', L) = 0 \tag{2.52}$$

$$\mathcal{G}(x, x, x', y') = \mathcal{G}(x, y, x', x') = 0 \tag{2.53}$$

The computation of the density function of the hole probabilities requires the computation of the Green function. This is done in two steps. First notice that

$$\mathcal{G}(x, y, x', y') = \mathcal{G}_{\square}(x, y, x', y') - \mathcal{G}_{\square}(y, x, x', y') \tag{2.54}$$

where $\mathcal{G}_{\square}(x, y, x', y')$ is the Green function of the Dirichlet problem defined in the interior of the square $0 \leqslant x \leqslant L$, $0 \leqslant y \leqslant L$. One can construct $G_{\square}$ easily by using reflection techniques. All that one needs to know is the

Green function of the Dirichlet problem defined on the entire plane (with boundaries at infinity). We denote the last-mentioned function with $g(x, y, x', y')$. Summing up, we get

$$\mathcal{G}(x, y, x', y') = \sum_{\alpha,\beta=\pm 1} \alpha\beta \sum_{i,j=-\infty}^{+\infty} [g(\sqrt{(x-2iL-\alpha x')^2+(y-2jL-\beta y')^2}) - g(\sqrt{(y-2iL-\alpha x')^2+(x-2jL-\beta y')^2})] \tag{2.55}$$

Once the density function $\hat{\Omega}(x, y)$ is known, one can compute expectation values of observables in the steady state. The local particle density is given by

$$\rho(x) = \lim_{y \to x} \frac{1-\{\exp[\frac{1}{2}\hat{r}(x+y)]\}\,\hat{\Omega}(x, y)}{y-x} = -\frac{\partial}{\partial y}\Omega^c(x, y)\bigg|_{y=x} \tag{2.56}$$

We also give a closed formula for the computation of the connected two-point function:

$$G^c(x, y) = \langle n_x n_y \rangle - \langle n_x \rangle \langle n_y \rangle \tag{2.57}$$

Here n_x denotes the particle number operator at site x. Using the factorization properties of the two-hole probability function mentioned in refs. 10 and 11, it is easy see to that in the continuum limit we have

$$G^c(x, y) = \frac{\partial}{\partial x}\Omega^c(x, y)\frac{\partial}{\partial y}\Omega^c(x, y) - \Omega^c(x, y)\frac{\partial^2\Omega^c(x, y)}{\partial x\,\partial y} \tag{2.58}$$

2.3.1. The Scaling Limit in the Symmetric Case ($q=1$). In the case of symmetric diffusion the differential equation (2.46) reduces to a Laplace equation. The Green function can be obtained from (2.55) by replacing $g(u)$ with $(1/2\pi)\ln u$.

Let us consider for simplicity first the case of an *infinite particle input* rate ($\hat{p}=\infty$). In this case the hole density function is zero for $x=0$ [see Eq. (2.47)]. We are left with

$$\Omega^c_\infty(x, y) = \int_0^L du \left(\frac{\partial}{\partial x'} - \frac{\partial}{\partial y'}\right)\mathcal{G}(x, y, x', y')\bigg|_{x'=y'=u} - \int_0^L dx' \frac{x'}{L}\frac{\partial}{\partial x'}\mathcal{G}(x, y, x', y')\bigg|_{y'=L} \tag{2.59}$$

Inserting Eq. (2.55), one is led to

$$\Omega^{c}_{\infty}(x,y)$$
$$= \sum_{\alpha,\beta=\pm 1} \alpha\beta \times \sum_{i,j=-\infty}^{+\infty} \left\{ \arctan \frac{\alpha(2i-x/L)-\beta(2j-y/L)}{(2i-x/L)^2+(2j-y/L)^2+\alpha(2i-x/L)+\beta(2j-y/L)} - \left[\beta\left(i-\frac{x}{2L}\right)+\alpha\left(j-\frac{y}{2L}\right)\right] \arctan \frac{\alpha+2i-x/L}{\beta+2j-y/L} \right\} \tag{2.60}$$

We see that the hole density function for $\hat{p}=\infty$ depends only on x/L and y/L. From Eq. (2.56) we obtain the local particle density in the stationary state for *infinite* particle input rate:

$$\rho_{\infty}(x) = \frac{2}{\pi L} \sum_{i,j=-\infty}^{+\infty} \frac{(x/L-2i)+(x/L-2j)}{(x/L-2i)^2+(x/L-2j)^2} \tag{2.61}$$

Defining $z=x/L$, we can rewrite Eq. (2.61) as

$$L\rho_{\infty}(x) = \Phi(z) \tag{2.62}$$

where

$$\Phi(z) = \frac{1}{\pi} \sum_{i,j=-\infty}^{+\infty} \frac{(z/2-i)+(z/2-j)}{(z/2-i)^2+(z/2-j)^2}$$
$$= \frac{\sinh(\pi z)+\sin(\pi z)}{\cosh(\pi z)-\cos(\pi z)} + \sum_{k=1}^{+\infty} \left\{ \frac{\sinh[2\pi(z/2-k)]+\sin(\pi z)}{\cosh[2\pi(z/2-k)]-\cos(\pi z)} + (k \leftrightarrow -k) \right\} \tag{2.63}$$

The function $\Phi(z)$, called the scaling function, is odd and periodic with period 2. In the limit $z \to 0$ the function diverges like $2/\pi z$ [the dominant contribution is given by the first term in the second line of (2.63)]. For $z \to 1$, $\Phi(z)$ approaches the value 1, but the value itself at the point $z=1$ is $\Phi(1)=0$. So the function is discontinuous for all integer arguments.

We consider now the case of an arbitrary input rate $\hat{p}$ and look at the scaling regime (z fixed, $L \to \infty$). If $\hat{p}$ is finite, one picks up another contribution to the hole density function coming from the integration along

the boundary segment ($x=0$, $0 \leqslant y \leqslant L$) in (2.50). The difference between the values of the hole density function corresponding to infinite and finite input rates is

$$\Omega^c_{\infty}(x, y) - \Omega^c_{\hat{p}}(x, y) = \int_0^L dy'\, \Omega^c_{\hat{p}}(0, y') \frac{\partial}{\partial x'} \mathcal{G}(x, y, x', y') \bigg|_{x'=0} \tag{2.64}$$

We are here interested in the scaling and thermodynamic limit. For large values of the lattice length L, $\Omega^c_{\hat{p}}(0, y')$ behaves like $\exp[-y'(\hat{p})^{1/2}]$. We expand the derivative of the Green function in Eq. (2.64) near $y'=0$ and get

$$\begin{aligned}
&\Omega^c_{\infty}(x, y) - \Omega^c_{\hat{p}}(x, y) \\
&\quad = \frac{16}{\pi} \sum_{i,j=-\infty}^{+\infty} \frac{(x/L-2i)(y/L-2j)[(y/L-2j)^2-(x/L-2i)^2]}{[(y/L-2j)^2+(x/L-2i)^2]^4} \\
&\qquad \times \int_0^1 \frac{\sinh[(\hat{p})^{1/2} L(1-u)]}{\sinh[(\hat{p})^{1/2} L]} (u^3 + O(u^7))\, du
\end{aligned}$$

It is easy to see that in the finite-size scaling limit one gets

$$\Phi_{\hat{p}}(z) = \Phi(z) + \frac{1}{L^4} \Phi^{\mathrm{corr}}(z) + O\left(\frac{1}{L^8}\right) \tag{2.65}$$

The first finite-size scaling correction function is

$$\begin{aligned}
\Phi^{\mathrm{corr}}(z) = &\frac{3}{\pi \hat{p}^2} \sum_{i,j=-\infty}^{+\infty} \left(\frac{z}{2} - i\right) \\
&\times \frac{(z/2-i)^4 - 10(z/2-i)^2 (z/2-j)^2 + 5(z/2-j)^4}{[(z/2-i)^2+(z/2-j)^2]^5}
\end{aligned} \tag{2.66}$$

So we proved that in the scaling limit the particle density function scales. The scaling function $\Phi(z)$ given by Eq. (2.63) is independent of the input rate. We get finite-size corrections of order L^{-4} for finite input rates.

In Fig. 2 we show the function (solid curve)

$$F(z) = \frac{\pi z}{2} \Phi(z) \tag{2.67}$$

[with this definition $F(0)=1$] together with finite-lattice calculations [see Eqs. (2.29) and (2.20)] obtained for $L=2000$ ($p=1$) and for $L=800$ ($p=\infty$). We have given this figure for two reasons. First we observe that

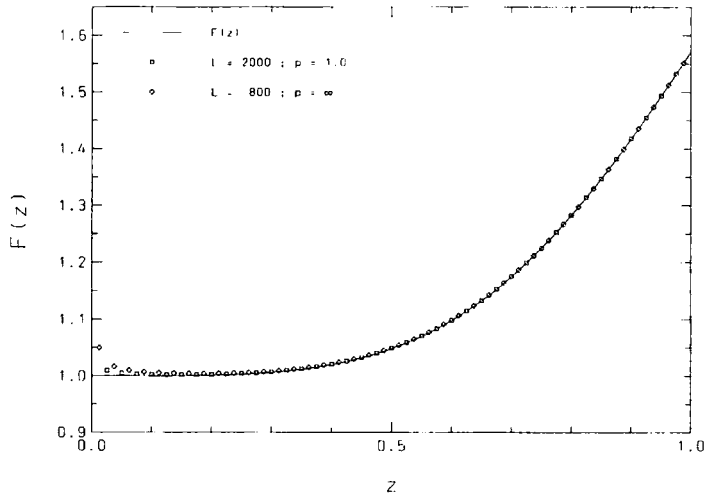

Fig. 2. The function $F(z)$ defined by Eq. (2.67) (solid curve) compared to lattice calculations for $L=2000$ ($p=1.0$) and $L=800$ ($p=\infty$).

the scaling function has a nontrivial behavior at the opened end of the system ($z \propto 1$). Next, although the scaling function was computed in the continuum limit, it applies to the lattice, too.

Let us consider the *thermodynamic limit* $L \to \infty$, x fixed. Using Eqs. (2.56) and (2.55) (from the multiple sum of the latter we take only the terms corresponding to $i=j=0$), one can show that

$$\rho(x) = \frac{2}{\pi x} - \frac{12}{\pi \hat{p}^2 x^5} + \frac{5040}{\pi \hat{p}^4 x^9} + O(p^{-6} x^{-13}) \tag{2.68}$$

The asymptotic behavior (for large values of x) of the one-point function in the thermodynamic limit (2.68) can be also obtained from the scaling behavior (2.65) in the limit $z \to 0$. The result (2.68) is consistent with the expansion for the stationary concentration profile on a discrete lattice (2.38). The only difference is that in the continuum limit all contributions $1/x^i p^j$ with $i > 2j+1$ scale like λ^{i-2j-1} and therefore vanish in the limit of vanishing lattice spacing $\lambda \to 0$.

We mention one last result concerning the connected two-point function. In the thermodynamic limit one can see[11] that the hole probability density for infinite input rate is

$$\Omega^c_\infty(x, y) = \frac{4}{\pi} \arctan\left(\frac{x}{y}\right) \tag{2.69}$$

Using (2.58), one gets the following expression for the connected two-point-function:

$$G^c(x, x+d) = -\frac{16}{\pi^2}\frac{1}{x^2}\frac{1+v-v(2+v)\arctan[1/(1+v)]}{(2+2v+v^2)^2} \tag{2.70}$$

in the infinite-input-rate case. On the right-hand side of (2.70) we denoted d/x with v. Notice again the algebraic falloff.

2.3.2. Bias to the Right ($\hat{r}>0$). Writing the Fourier transform of (2.51), one gets

$$g(u) = -\frac{1}{(2\pi)^2}\int_0^\infty \frac{k\,dk}{k^2+\hat{r}^2/2}\int_0^{2\pi} e^{-iku\cos\theta}\,d\theta \tag{2.71}$$

Thus the Green function of the problem defined on the entire plane is [see formulas (9.6.16) in ref. 13 and (6.532.4) in ref. 14]

$$g(u) = -\frac{1}{2\pi}K_0\left(\sqrt{\frac{\hat{r}^2}{2}}u\right) \tag{2.72}$$

We use the standard notation K_i, $i=0, 1, 2,...$, for the modified Bessel functions.

In Appendix B we prove that in the thermodynamic limit the asymptotic behavior of the particle density is given by

$$\rho(x) = \sqrt{\frac{\hat{r}}{2\pi x}} + \frac{1}{4\sqrt{2\pi\hat{r}}}\left(\frac{11}{2}-\frac{\hat{r}^4}{\hat{p}^2}\right)\frac{1}{x^{3/2}} + O(x^{-5/2}) \tag{2.73}$$

The leading term is the continuum analogue of the one appearing in Eq. (2.42) and is independent of the input rate.

We conclude this section with some remarks concerning the influence of the right boundary on the particle density.

As opposed to the symmetric case, one can check that for biased diffusion to the right the behavior of the one-point function in the thermodynamic limit is identical with the one in the scaling limit. One can give a qualitative explanation. In the stationary state, near the right boundary, the density function can be approximated by the one given by a single particle occupying the whole lattice (a random walker)

$$c(y) = \begin{cases} q^{-2y}\dfrac{1-q^{-2}}{1-q^{-2L}} & \text{for} \quad q \neq 1 \\ \dfrac{1}{L} & \text{for} \quad q = 1 \end{cases} \tag{2.74}$$

where $y = L - x$.

For biased diffusion to the right the density decays exponentially in y. So the influence of the right boundary is of short range and is not seen in the scaling limit.

For $q=1$ (or $\hat{r}=0$) the influence of the right boundary is much stronger. The density determined by a random walker near the right end of the lattice is constant $(1/L)$ and greater than the one obtained through the extrapolation of Eq. (2.38), $2/\pi L$. This explains the linear behavior of the reduced scaling function $F(z)$ for $z \to 1$ (see Fig. 2).

One can also notice from the y and L dependence of $c(y)$ that one has a characteristic length scale $\Lambda = (2 \ln q)^{-1}$, which is related to the inverse mass seen in the spectrum of the Hamiltonian [see Eq. (2.18)]. This observation is very interesting, since it clarifies a puzzle which goes through this paper: how can a system with massive excitations in the time direction show an algebraic and, as we shall see in the next section, universal behavior? The answer is that one looks at the concentration in the "wrong" way following the x dependence (away from the source) and not the y dependence (away from the open end). The discovery that this "wrong" way exists is probably the main achievement of this paper.

3. NUMERICAL VERIFICATION OF THE UNIVERSALITY HYPOTHESIS

In this section we present the results of Monte Carlo simulations. The details are given in Appendix C. We restrict the study to cases for which $p_R = 0$ and $r \geqslant 0$. We start with the symmetric diffusion case ($q=1$ or $r=0$). First we look at the density profile ($1 \ll x \ll L$). As suggested by Eq. (2.38), we fit the data by the function

$$c(x) = \frac{K_1}{x} + \frac{K_2}{x^2} + \frac{K_3}{x^3} \tag{3.1}$$

When making the fits (by using the χ^2 method), we took points $x \in [L/10, L/2]$ in order to avoid finite-size effects. The estimates for K_1 and K_2 for various input and bulk rates are given in Table I. The data presented here were obtained taking lattices of size $L = 1000$.

We notice that K_1 is everywhere close to the value obtained in the fermionic case ($s=2$, $t=0$), namely $K_1 = 2/\pi \simeq 0.637$. The values of K_2 are different if the bulk rates are different, but as in the fermionic case, they do not depend on the input rate.

Since the leading term of the density profile is compatible with universality, one can go one step further and check if the scaling function $\Phi(z)$

Table I. Estimates of the Coefficients K_1 and K_2 of the Expression (3.1) for Various Input and Bulk Rates

s	t	p	K_1	K_2
0.50	0	1	0.635 ± 0.001	10.2 ± 0.2
0.50	0	∞	0.639 ± 0.004	9.8 ± 0.8
0.50	-0.2	1	0.640 ± 0.010	16 ± 5
0.50	-0.2	∞	0.640 ± 0.010	13 ± 3
0.25	0	1	0.637 ± 0.002	22 ± 4
0.25	0	∞	0.632 ± 0.002	24.4 ± 0.4
0.40	-0.2	1	0.638 ± 0.002	11 ± 2
0.40	-0.2	∞	0.642 ± 0.004	10.4 ± 0.6

given by Eq. (2.63) in the fermionic case is also universal. This function was obtained taking $x/L = z$ fixed (x and L large):

$$\lim_{L \to \infty} Lc(z, L) = \Phi(z) \tag{3.2}$$

We define the function

$$K(z, L) = \frac{Lc(z, L)}{\Phi(z)} - 1 \tag{3.3}$$

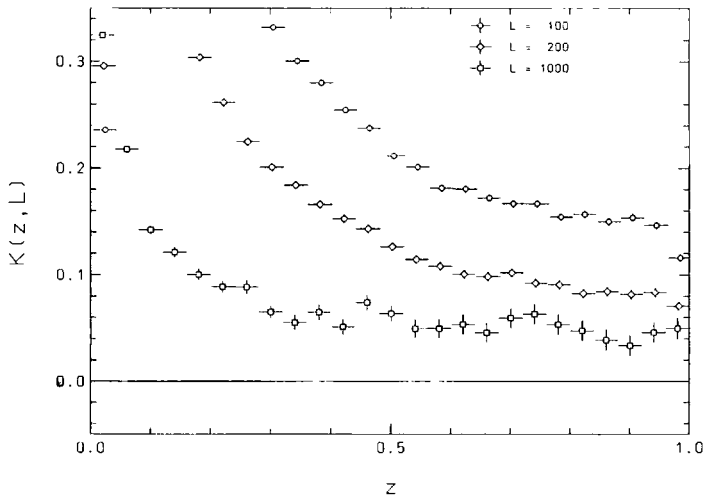

Fig. 3. The L dependence of the $K(z, L)$ function defined by Eq. (3.3) for $p = 1.0$, $s = 0.5$, $r = t = 0$. If the scaling function is universal, $K(z, L)$ should vanish in the thermodynamic limit. Monte Carlo simulations.

which measures the deviation from universality and the finite-size effects. In Fig. 3 we give the data in the case $p=1$, $s=0.5$, $t=0$ for three lattice sizes. One notices that with increasing lattice size, $K(z, L)$ decreases, as it should. One should mention that for $z=0$, $K(z, L)$ has to go to zero in the limit $L \to \infty$ because of the universality of K_1 in Eq. (3.1) and the uniform convergence of $\Phi(z)$, as proven in the fermionic case. Thus the relatively large values of $K(z, L)$ observable in Fig. 3 for small values of z should not be a subject of concern. We have also done other simulations (not shown in Fig. 3) for other input rates, which show the same pattern.

In Fig. 4, $K(z, L)$ is shown for various input and coagulation rates for a lattice of length $L=1000$. As one can see, $K(z, L)$ is small everywhere (for small values of z the convergence is slow, but, as mentioned above, for $z=0$ universality was checked already).

We now consider the asymmetric diffusion case ($q>1$). As suggested by Eq. (2.42), we fit the Monte Carlo data by the function

$$c(x) = K'_{1/2} x^{-1/2} + K'_1 x^{-1} + K'_{3/2} x^{-3/2} \tag{3.4}$$

We choose $q=\sqrt{2.5}$ (which corresponds to $r=0.857$), in which case we get from Eq. (2.42) $K'_{1/2}=\sqrt{3/(7\pi)} \simeq 0.369$. Notice that we have allowed a term $\sim x^{-1}$ not present in Eq. (2.42). The data were collected for $L=1000$ and the results are shown in Table II.

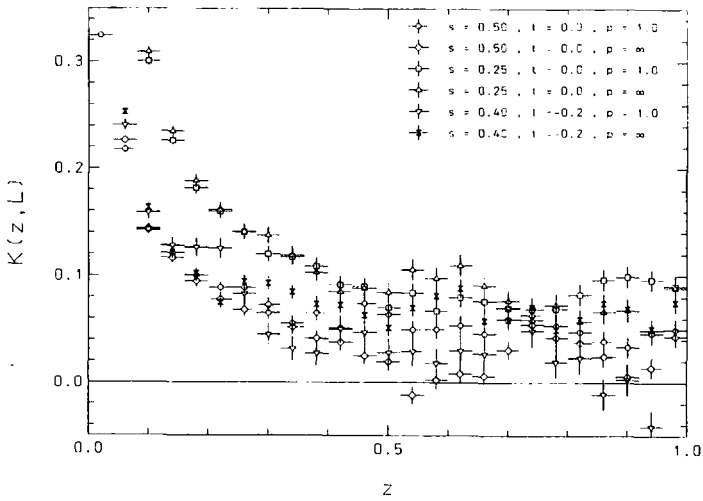

Fig. 4. The $K(z, L)$ function for $L=1000$, $r=0$, and different input and coagulation rates. Monte Carlo simulations.

Table II. Coefficients $K'_{1/2}$ and K'_1 of the Expansion (3.4) for Various Input and Coagulation Rates[a]

s	t	p	$K'_{1/2}$	K'_1
1.000	0.429	1	0.370 ± 0.003	0.10 ± 0.01
1.000	0.429	∞	0.368 ± 0.002	0.11 ± 0.01
0.500	0.214	1	0.368 ± 0.003	0.90 ± 0.04
0.500	0.214	∞	0.369 ± 0.004	0.82 ± 0.07
0.250	0.107	1	0.369 ± 0.002	2.12 ± 0.02
0.250	0.107	∞	0.369 ± 0.002	2.09 ± 0.02
0.361	−0.181	1	0.368 ± 0.001	1.27 ± 0.02
0.361	−0.181	∞	0.369 ± 0.003	1.25 ± 0.04

[a] All data are for $q = \sqrt{2.5}$ ($r = 0.857$).

As can be seen from this table, the coefficient $K'_{1/2}$ is unchanged (universal). The K'_1 is independent of the input, but depends on the bulk rates [similar to the K_2 coefficient in Eq. (3.1)]. Finally we notice that the values of K'_1 get smaller if we approach the fermionic case ($r = t = 0.857$, $s = 2$).

To sum up, in the symmetric diffusion case the Monte Carlo data suggest that the large-x behavior and the scaling function are universal: they are independent of the c_L, c_R, and p rates. In the asymmetric diffusion case, the large-x behavior is also universal.

4. CONNECTION WITH OTHER MODELS

It is well known that the coagulation model $A + A \to A$ and the annihilation model $A + A \to \varnothing$ belong to the same universality class. This equivalence is due to the existence of a local similarity transformation between their time evolution operators.[15] We now use this transformation in order to apply the results of the preceding sections to a coagulation–annihilation model (called CA) with boundary effects, which is defined by the following processes and rates:

$A\varnothing \to \varnothing A$	diffusion to the right at rate $\tilde{a}_R$
$\varnothing A \to A\varnothing$	diffusion to the left at rate $\tilde{a}_L$
$AA \to \varnothing A$	coagulation to the right at rate $\tilde{c}_R$
$AA \to A\varnothing$	coagulation to the left at rate $\tilde{c}_L$
$AA \to \varnothing\varnothing$	pair annihilation at rate $\tilde{\kappa}$

In addition, particles are absorbed (desorbed) at rate $\tilde{\gamma}$ ($\tilde{\delta}$) at the left boundary. In the configuration basis the time evolution operator $H^{\mathrm{CA}} = I_1^{\mathrm{CA}} + \sum_{n=1}^{L-1} H_{n,n+1}^{\mathrm{CA}}$ is given by

$$H_{n,n+1}^{\mathrm{CA}} = \begin{pmatrix} 0 & 0 & 0 & -\tilde{\kappa} \\ 0 & \tilde{a}_L & -\tilde{a}_R & -\tilde{c}_R \\ 0 & -\tilde{a}_L & \tilde{a}_R & -\tilde{a}_L \\ 0 & 0 & 0 & \tilde{\kappa}+\tilde{c}_R+\tilde{c}_L \end{pmatrix}, \qquad I_1^{\mathrm{CA}} = \begin{pmatrix} \tilde{\gamma} & -\tilde{\delta} \\ -\tilde{\gamma} & \tilde{\delta} \end{pmatrix} \tag{4.1}$$

As shown in ref. 15, the coagulation model (1.3) and the generalized annihilation model (4.1) are related by a local similarity transformation $H^{\mathrm{CA}} = UH^{\mathrm{coag}}U^{-1}$,

$$U = u \otimes u \otimes \cdots \otimes u = u^{\otimes L}, \qquad u = \begin{pmatrix} 1 & 1-a \\ 0 & a \end{pmatrix} \tag{4.2}$$

where a is some parameter. The rates of the coagulation–annihilation model are related to those of the original coagulation model by

$$\begin{aligned} \tilde{a}_{L,R} &= a_{L,R} \\ \tilde{c}_{L,R} &= c_{L,R} + \frac{1-a}{a}(a_{R,L} - a_{L,R} - c_{R,L}) \\ \tilde{\kappa} &= \frac{1-a}{a}(c_L + c_R) \\ \tilde{\gamma} &= ap \\ \tilde{\delta} &= (1-a)\,p \end{aligned} \tag{4.3}$$

Notice that if the original model had only input of particles, the equivalent coagulation–annihilation model has both input and output of particles. Because of the simplicity of the transformation, the n-point density–density correlation functions in the coagulation and coagulation–annihilation model are related by

$$\langle \tau_{j_1} \tau_{j_2} \cdots \tau_{j_n} \rangle^{\mathrm{CA}} = a^n \langle \tau_{j_1} \tau_{j_2} \cdots \tau_{j_n} \rangle^{\mathrm{coag}} \tag{4.4}$$

5. CONCLUSIONS

In the present paper we investigated the coagulation–diffusion model with particle input at one boundary using both analytical and numerical methods. The results show that spatial long-range correlations play an

essential role and that some physical properties are universal with respect to the input and the coagulation rates.

We started our analysis with a simple space-dependent mean-field approximation. It predicts algebraic behavior of the particle density in the stationary state for both symmetric and biased diffusion. However, rigorous results require an exact solution of the problem. To this end we solved the full problem by using the IPDF formalism. This formalism can be used only if the coagulation and diffusion rates coincide, a case which corresponds to free fermions in the Hamiltonian language. The large-x behavior (x is the distance to the source) of the particle density was computed in the thermodynamic limit both for the lattice and the continuum version and the results were compared. These painful calculations were done for symmetric and asymmetric diffusion. In the case of symmetric diffusion the scaling limit (x/L fixed, L is the lattice length) was obtained.

Monte Carlo simulations show that the coefficients of the leading terms of the asymptotic expansion of the density in the thermodynamic limit are universal: they are independent of the input rates (this was to be expected from mean-field) and on the coagulation rates. The scaling function is also universal in the symmetric case. It is trivial in the asymmetric case (it coincides with the leading term of the large-x behavior of the density). These results were to be expected from common sense in the symmetric case, but not for the asymmetric case. The reason is the following: the relaxation spectrum of the system is massless in the first, but massive in the second case. There exists a myth according to which if there are lengths in the time evolution, there should be lengths in the space correlations. A counterexample can be found, however, in the kinetic Ising model.[8] In the coagulation–diffusion model the picture is more perverse: if one looks at the concentration starting at the opened end, one finds an exponential falloff, but an algebraic and universal behavior if we start at the source end.

The message of this paper can be extended to the problem in which we add pair annihilation in the bulk and an output of particles at the source. What is still missing is a proof of universality which goes beyond numerical checks. This can be done using field-theoretic methods à la Cardy.[16,17]

APPENDIX A. PROOF OF THE SOLUTION IN THE THERMODYNAMIC LIMIT

In this appendix we prove the integral representation for the one-hole probabilities in the thermodynamic limit (2.33):

$$\Omega(x, y) = 1 - \frac{q^{x+y}}{2\pi i} \int_{-\gamma}^{+\gamma} dz \left(\frac{1}{z} - \frac{z}{z^2 + p^2} \right) (\mu_z^x \mu_{-z}^y - \mu_z^y \mu_{-z}^x) \qquad \text{(A.1)}$$

Instead of deriving this formula from the finite-size solutions (2.24)–(2.26) by taking $L \to \infty$, it is much simpler to prove that Eq. (A.1) is a solution of the one-hole equations (2.1)–(2.4). We first notice that $\Omega(x, x) = 1$ because of the antisymmetry of the integrand. In order to verify the bulk equation (2.1), let us introduce the notation $g(x, y, z) = q^{x+y}(\mu_z^x \mu_{-z}^y - \mu_z^y \mu_{-z}^x)$. Using Eq. (2.31), one can show that

$$qg(x-1, y, z) + q^{-1} g(x+1, y, z) + qg(x, y-1, z) + q^{-1} g(x, y+1, z)$$
$$= 2(q + q^{-1})\, g(x, y, z) \tag{A.2}$$

This relation implies that Eq. (A.1) satisfies the bulk equation (2.1). The last step is to verify the left boundary condition (2.2). Obviously it is equivalent to proving that

$$h(y) = q\Omega(0, y-1) + q^{-1}\Omega(0, y+1) - (q + q^{-1} + p)\,\Omega(0, y)$$
$$= -p + \frac{p^2 q^y}{2\pi} \int \frac{dz}{z} \left(\frac{\mu_z^y}{z + ip} + \frac{\mu_{-z}^y}{z - ip} \right) \tag{A.3}$$

is equal to zero for all $y = 1, 2, \ldots, \infty$. For $y = 0$ we get

$$h(0) = -p + \frac{p^2}{2} \int_{-\pi}^{+\pi} dz \, \frac{1}{z^2 + p^2} = 0 \tag{A.4}$$

For $y = 1$ one has to solve the integrals

$$h(1) = -p + \frac{qp^2}{2\pi} \left(\int_{-\pi}^{+\pi} dz \, \frac{\mu_z + \mu_{-z}}{z^2 + p^2} - \int_{-\pi}^{+\pi} \frac{dz}{z} \, \frac{ip(\mu_z - \mu_{-z})}{z^2 + p^2} \right) \tag{A.5}$$

by standard integration techniques in the complex plane. It turns out that all contributions cancel except at $z = 0$ in the second integral, so that $h(1) = 0$. Using Eq. (2.31), it is now easy to derive the recurrence relation

$$q^{-1} h(y) + qh(y-2) = (q + q^{-1})\, h(y-1) \tag{A.6}$$

so that $h(y) = 0$ for $y = 2, 3, \ldots, \infty$ follows by induction. This completes the proof of Eq. (A.1).

Let us finally consider the case of infinite input rate, where Eq. (A.1) reduces to

$$\Omega(x, y) = 1 - \frac{q^{x+y}}{2\pi i} \int_{-\pi}^{+\pi} \frac{dz}{z} \, (\mu_z^x \mu_{-z}^y - \mu_z^y \mu_{-z}^x) \tag{A.7}$$

This expression turns out to be a combination of elliptic integrals. This allows us to compute the particle concentration exactly, although the expressions become very complicated as x and y increase. For example, the particle concentration in the steady state at the first four sites is given by

$$c(1)=1 \tag{A.8}$$

$$c(2)=\frac{2}{3\pi}\left[(q^2+1)(1+6q^2+q^4)\,\mathbf{E}-(q^2+1)(q^2-1)^2\,\mathbf{K}\right]-q^2-2q^4 \tag{A.9}$$

$$c(3)=\frac{2}{15\pi}\left[(q^2+1)(4-15q^2-34q^4-15q^6+4q^8)\,\mathbf{E}\right.$$
$$\left.-(q^2+1)(q^2-1)^2(4-15q^2+4q^4)\,\mathbf{K}\right]+3q^4-2q^6 \tag{A.10}$$

$$c(4)=\frac{4}{105\pi}\left[(q^2+1)(12-28q^2+45q^4+238q^6+45q^8-28q^{10}+12q^{12})\,\mathbf{E}\right.$$
$$\left.-(q^2+1)(q^2-1)^2(12-28q^2+69q^4-28q^6+12q^8)\,\mathbf{K}\right]-3q^6-4q^8 \tag{A.11}$$

where

$$\mathbf{E}=\int_0^{\pi/2} d\theta\left(1-\frac{4}{(q+q^{-1})^2}\sin^2\theta\right)^{1/2} \tag{A.12}$$

$$\mathbf{K}=\int_0^{\pi/2} d\theta\left(1-\frac{4}{(q+q^{-1})^2}\sin^2\theta\right)^{-1/2} \tag{A.13}$$

are elliptic integrals of the first kind.

APPENDIX B. THE ONE-POINT FUNCTION FOR BIASED DIFFUSION TO THE RIGHT IN THE CONTINUUM LIMIT

In this appendix we give a proof of Eq. (2.73). We concentrate on the thermodynamic limit of models in which the particle motion is subject to a drift pointing away from the source which is situated at the left boundary ($x=0$) and we are interested in the large-x behavior of the density. The starting point is the contour integral (2.50). In the thermodynamic limit the Green function of the Dirichlet problem is defined by the $i=j=0$ term of

the multiple sum of (2.55). We are left with two contributions to the hole density function,

$$\Omega^c(x, y) = \Omega^c_\infty(x, y) + \Omega^c_p(x, y) \tag{B.1}$$

The first one comes from the integration along the diagonal boundary half-line[4] ($0 \leqslant x' = y' < \infty$),

$$\Omega^c_\infty(x, y) = \frac{|\hat{r}|}{2\pi} \sum_{\alpha,\beta = \pm 1} (\alpha y - \beta x) \int_0^\infty \frac{K_1(|\hat{r}|\, r_1)}{r_1} e^{-\hat{r}[a - (x+y)/2]}\, da \tag{B.2}$$

Here

$$r_1 = \left[\left(a - \frac{ax + \beta y}{2} \right)^2 + \left(\frac{\alpha x - \beta y}{2} \right)^2 \right]^{1/2}$$

This is the hole density function in the case of an infinite input rate.

The second contribution comes from the integration along the left boundary half-line ($0 \leqslant y' < \infty$, $x' = 0$) and is $\hat{p}$ dependent:

$$\begin{aligned} \Omega^c_p(x, y) = {} & \frac{|\hat{r}|}{\sqrt{2\pi}} \sum_{\alpha = \pm 1} \alpha \exp \frac{\hat{r}(x+y)}{2} \\ & \times \int_0^\infty \left\{ y \frac{K_1(|\hat{r}|\, r_2/\sqrt{2})}{r_2} - x \frac{K_1(|\hat{r}|\, r_3/\sqrt{2})}{r_3} \right\} \\ & \times \exp \left[- \left(\frac{\hat{r}^2}{4} + \hat{p} \right)^{1/2} a \right] da \end{aligned} \tag{B.3}$$

where $r_2 = [(a - \alpha x)^2 + y^2]^{1/2}$ and $r_3 = [(a - \alpha y)^2 + x^2]^{1/2}$.

The density profile is determined by the hole density function in the limit $y \to x$ [see Eq. (2.56)]. The behavior of the integrands appearing in (B.2) and (B.3) is given by terms of the form $K_1(u)/u$. For $u \to 0$ the modified Bessel functions diverge like $K_\nu(u) \sim u^{-\nu}$ [for $\mathrm{Re}(\nu) > 0$]. The only dangerous term is the one containing r_1, which vanishes for $y \to x$ and $a \to x$ when $\alpha = \beta = 1$. The corresponding term in (B.2),

$$\begin{aligned} \Omega^c_0(x, y) = {} & \frac{|\hat{r}|(y - x)}{2\pi} \int_0^\infty \frac{K_1(|\hat{r}| \sqrt{(a - (x+y)/2)^2 + (x-y)^2/4})}{\sqrt{(a - (x+y)/2)^2 + (x-y)^2/4}} \\ & \times e^{-\hat{r}[a - (x+y)/2]}\, da \end{aligned} \tag{B.4}$$

[4] We note that the derivatives of the Bessel functions with respect to their argument are $K_0'(u) = -K_1(u)$ and $K_1'(u) = -\frac{1}{2}[K_0(u) + K_2(u)]$.

determines the asymptotic behavior of the particle concentration in the thermodynamic limit. We start with this term. We use the fact that $K_1(\sqrt{u})/\sqrt{u}$ is the Laplace transform of $e^{-1/(4t)}$ [see Eq. (29.3.122) in ref. 13]. The Eq. (B.4) can be rewritten

$$\Omega_0^c(x, y) = \hat{r}^2 \frac{y-x}{2\pi} \int_0^\infty \exp\left[-t\hat{r}^2 \left(\frac{x-y}{2}\right)^2 \right] dt$$
$$\times \int_{-(x+y)/2}^{\infty} \exp\left[-t\left(\hat{r}a + \frac{1}{2t}\right)^2 \right] da \tag{B.5}$$

After integrating over the variable a, we get

$$\Omega_0^c(x, y) = 1 - \hat{r}\frac{y-x}{2\sqrt{\pi}} \int_0^\infty \exp\left[-t^2\hat{r}^2 \left(\frac{x-y}{2}\right)^2 \right]$$
$$\times \operatorname{erfc}\left(t\hat{r}\frac{x+y}{2} - \frac{1}{2t} \right) dt \tag{B.6}$$

Here erfc stands for the complementary error function. From (2.56) we get that the contribution of $\Omega_0^c(x, y)$ to the particle density is

$$\rho_0(x) = \frac{\hat{r}}{2\sqrt{\pi}} \int_0^\infty \operatorname{erfc}\left(t\hat{r}x - \frac{1}{2t} \right) dt \tag{B.7}$$

With the change of variable

$$t = \frac{\omega + \sqrt{\omega^2 + 2\hat{r}x}}{2\hat{r}x} \tag{B.8}$$

we get

$$\rho_0(x) = \frac{1}{2\sqrt{\pi}\, x} \left(\int_0^\infty \left(1 - \frac{\omega}{\sqrt{\omega^2 + 2\hat{r}x}} \right) d\omega \right.$$
$$\left. + \int_0^\infty \frac{\omega}{\sqrt{\omega^2 + 2\hat{r}x}} \operatorname{erfc}(\omega)\, d\omega \right) \tag{B.9}$$

After integrating by parts one gets

$$\rho_0(x) = \frac{1}{\pi x} \int_0^\infty \sqrt{\omega^2 + 2\hat{r}x}\, e^{-\omega^2}\, d\omega \tag{B.10}$$

Expanding in powers of ω^2/x, we finally obtain

$$\rho_0(x) = \sqrt{\frac{\hat{r}}{2\pi x}} + \frac{1}{8\sqrt{2\pi\hat{r}}}\frac{1}{x^{3/2}} + O(x^{-5/2}) \tag{B.11}$$

The rest of the hole density function

$$\Omega^c_{\text{rest}}(x, y) = \Omega^c(x, y) - \Omega^c_0(x, y) \tag{B.12}$$

gives also a contribution to the particle density

$$\rho_{\text{rest}}(x) = -\frac{\partial}{\partial y}\Omega^c_{\text{rest}}(x, y)\bigg|_{y=x} \tag{B.13}$$

In all the integrals contributing to Ω^c_{rest}, the arguments of the Bessel functions (r_i, $i = 1, 2, 3$) are greater than x (or y). We can thus use the asymptotic expansions of $K_\nu(u)$ and replace these functions with $\exp(-u)\cdot\sqrt{\pi/(2u)}$. One obtains an integral expression of $\rho_{\text{rest}}(x)$. Due to the exponential falloff of the integrands appearing in (B.13), one can expand them in powers of a/x (where a is the integration variable). After some computations one gets that for $x \to \infty$, $\rho_{\text{rest}}(x)$ decays like $x^{-3/2}$.

Summing up, we get the following formula for the asymptotic behavior of the density profile:

$$\rho(x) = \sqrt{\frac{\hat{r}}{2\pi x}} + \frac{1}{4\sqrt{2\pi\hat{r}}}\left(\frac{11}{2} - \frac{\hat{r}^4}{\hat{p}^2}\right)\frac{1}{x^{3/2}} + O(x^{-5/2}) \tag{B.14}$$

We notice that the leading term is independent of the input rate $\hat{p}$, but the next to leading term is $\hat{p}$ dependent.

APPENDIX C. DETAILS ON THE MONTE CARLO SIMULATIONS

In this appendix we explain how we did the simulations of the coagulation–diffusion model with particle input at one boundary ($p_R = 0$). We can simplify the notation and use the symbol p instead of p_L for the input rate.

The simplest way to simulate reaction–diffusion models is to use a Monte Carlo algorithm with random sequential updates. However, this algorithm is not very efficient for the present problem since particle densities are very low and therefore most of the updates take place at empty

sites. This is why we used a different method in which the positions of the particles are stored rather than the occupation numbers of the sites (for details see ref. 18 and references therein). This "direct" method is much faster than the first one. It is defined as follows. At the beginning the lattice is empty. As long as the total number of particles in the system is 0, the following steps are repated:

- Choose randomly a number a, between 0 and 1.
- Occupy site 1 with a particle if $a \leqslant p\ \Delta t$.
- Leave the site unoccupied if $a > p\ \Delta t$.
- Increment the time $t \to t + \Delta t$.

The parameter Δt is a measure of the time discretization which is used.[18] After the first particle enters the system, the "direct" Monte Carlo algorithm is started:

- Choose randomly a *particle* and one of its neighboring sites.
- Update the configuration of the pair chosen before with the help of a random number and by considering the bulk reaction rates.
- Increment the time $t \to t + \Delta t/N$, where N is the current total number of particles in the system.
- If site 1 is empty, try to occupy it by comparing a random number with $p\ \Delta t/N$. If $p = \infty$, one keeps the site 1 occupied at all time steps.

In order to test the accuracy of the "direct" Monte Carlo method, we simulated some systems for which analytical data are available. The coincidence is very good. For $q = 1$ we used a lattice of length $L = 200$ and took $p = 1$ and $p = 0.01$. Only for the first 10–15 sites are the two sets of values for the density profile slightly different (the relative difference is less than 10%). For the other sites the difference between the two determinations of the density profile is zero in the limit of the numerical errors. We also compared data obtained for systems characterized by $q = \sqrt{2.5}$, $L = 20$ sites, and $p = 1$ and $p = 0.1$. Although the lattice length is small, the two sets of determinations of the density profiles coincide for all sites, in the limit of the errors.

The quality of the Monte Carlo determinations is higher in the case in which the particle diffusion is biased to the right in comparison with the $a_R \leqslant a_L$ case. This has two reasons. On one hand, in the $a_R > a_L$ case the total concentration of particles in the stationary state is larger than in the symmetric case. It is more likely to reproduce through simulations a distribution with a higher total number of particles. On the other hand, the relaxation of these system to the stationary state occurs much faster than

in the $a_R = a_L$ case since the time operator has massive excitations for $a_R \neq a_L$. This implies a smaller CPU time per run and thus the reduced numerical errors of the measurements are smaller.

It is well known that the quality of the Monte Carlo determinations is limited by the accuracy of the random number generator. If the number of steps requiring different random numbers is too high, at some point the generator produces correlated numbers. This limitation posed some problems in the case of symmetric diffusion for large lattices. This explains the unphysical oscillations presented by the data corresponding to $L = 1000$ in Figs. 3 and 4. The choice of a better random number generator implies the increase of the CPU time needed to perform the simulations.

Since we are interested in the stationary properties of the system, we stopped each simulation run at a value of $t = t_{\max}$ such that, at least in the time interval $[t_{\max}/3, t_{\max}]$, the average total number of particles is fluctuating around a constant value. We used a double-averaging technique. We took 100 equidistant time points between $[0.9t_{\max}, t_{\max}]$ and measured our observables in each of them. For each Monte Carlo run of the program we got a preliminary value by averaging over this 100 determinations. Afterward we averaged this preliminary value over all MC runs. The number of runs performed for each system was between 4000 and 50,000, depending on the lattice length. Due to CPU time limitations, the number of runs we performed decreases with the lattice length.

For the data presented in Figs. 3 and 4 we used coarse graining for obvious reasons; this is reflected in the horizontal error bars.

ACKNOWLEDGMENTS

We thank J. Cardy, B. Derrida, K. Krebs, I. Peschel, and G. M. Schultz for helpful hints and interesting discussions and P. A. Pearce for reading the manuscript. H.H. thanks the Minerva Foundation for financial support. H.S. expresses special thanks to E. Hegedüs for teaching him Green functions.

REFERENCES

1. R. Kroon, H. Fleurent, and R. Sprik, *Phys. Rev. E* **47**:2462 (1993).
2. K. Kang and S. Redner, *Phys. Rev. A* **30**:2833 (1984).
3. C. R. Doering and D. ben-Avraham, *Phys. Rev. A* **38**:3035 (1988); M. A. Burschka, C. R. Doering, and D. ben-Avraham, *Phys. Rev. Lett.* **63**:700 (1989); D. ben-Avraham, M. A. Burschka, and C. R. Doering, *J. Stat. Phys.* **60**:695 (1990); C. R. Doering, M. A. Burschka, and W. Horsthemke, *J. Stat. Phys.* **65**:953 (1991); D. ben-Avraham, *Mod. Phys. Lett. B* **9**:895 (1995).

4. R. J. Glauber, *J. Math. Phys.* **4**:294 (1963); D. Bedeaux, K. E. Schuler, and I. Oppenheim, *J. Stat. Phys.* **2**:1 (1970).
5. I. Peschel, V. Rittenberg, and U. Schultze, *Nucl. Phys. B* **430**:633 (1994).
6. T. Vicsek, P. Meakin, and F. Family, *Phys. Rev. A* **32**:1122 (1985); Z. Racz, *Phys. Rev. A* **32**:1129 (1985); H. Hayakawa, *J. Phys. A* **20**:L801 (1987); H. Takayasu, I. Hisikawa, and H. Taski, *Phys. Rev. A* **37**:3110 (1988); C. R. Doering and D. ben-Avraham, *Phys. Rev. Lett.* **62**:2563 (1989).
7. Z. Cheng, S. Redner, and F. Leyvraz, *Phys. Rev. Lett.* **62**:2321 (1989).
8. F. C. Alcaraz, M. Droz, M. Henkel, and V. Rittenberg, *Ann. Phys.* **230**:250 (1994).
9. K. Krebs, M. Pfannmüller, B. Wehefritz, and H. Hinrichsen, *J. Stat. Phys.* **78**:1429 (1995).
10. H. Hinrichsen, K. Krebs, and I. Peschel, *Z. Phys. B* **100**:105 (1996).
11. B. Derrida, V. Hakim, and V. Pasquier, *Phys. Rev. Lett.* **75**:751 (1995).
12. B. Derrida, *J. Phys. A* **28**:1481 (1995).
13. M. Abramowitz and I. A. Stegun, eds., *Handbook of Mathematical Functions* (Dover, New York, 1965).
14. I. S. Gradshteyn and I. M. Ryzhik, *Table of Integrals, Series, and Products*, 4th ed. (Academic Press, New York, 1965).
15. H. Simon, *J. Phys. A* **28**:6585 (1995).
16. B. P. Lee and J. Cardy, *J. Stat. Phys.* **80**:971 (1995).
17. J. Cardy, Private communication.
18. K. Krebs, M. Pfannmüller, H. Simon, and B. Wehefritz, *J. Stat. Phys.* **78**:1471 (1995).